# Automatic Detection of Mining Subsidence using InSAR and YOLOv11 Model

Lei Chen <sup>1</sup>, Jianyu Wang <sup>1</sup>, Ning Wang <sup>1</sup>, Siao Liu <sup>1</sup>, Hongwei Li <sup>1</sup>, Ye Tian <sup>1</sup>

<sup>1</sup> Satellite Communications Branch, China Telecom Co. Ltd., Beijing, China - chenlei.wx@chinatelecom.cn

**Keywords:** Object detection, Mining subsidence, InSAR, Deep learning, YOLOv11.

#### **Abstract**

Underground coal mining will cause serious ground subsidence and affect the life and property safety of surrounding residents. Deep learning provides the possibility to process a large amount of data information, and can provide an effective model based on a large number of training data to realize the automatic detection and recognition of a large number of data. In this paper, the YOLOV11 model is applied and a mining area in Shanxi Province was used for experimental research. The experiments show that an AI model suitable for automatic identification of subsidence area in Shanxi mining area is obtained, by training YOlOv11 model with limited SAR interferogram. The YOLOv11 model will also be applied to surface deformation caused by landslides and earthquakes in the future, so as to improve the identification efficiency of geological disasters and reduce the possible human and property losses caused by ground disasters.

### 1. Introduction

Underground coal mining will cause serious ground subsidence and affect the life and property safety of surrounding residents (Xue et al., 2012). It is very important to monitor the subsidence area of coal mining quickly and effectively, especially illegal coal mining activities (Hu et al., 2014). Traditional deformation monitoring technologies, such as GPS, GNSS, level, etc., can only obtain high-precision surface deformation information at the point location, which cannot meet the requirements of large-scale deformation monitoring, and the required manpower and material costs are high (Fan et al., 2018).

Interferometric synthetic aperture radar (InSAR) technology can extract a large range of high-precision surface deformation information, and is widely used in the monitoring of surface deformation caused by earthquakes, volcanoes, landslides and resource exploitation (Chen et al., 2016; Ma et al., 2022; Zhang et al., 2015). In order to remove the influence of factors such as spatiotemporal incoherence and atmospheric effect existing in InSAR technology, some scholars put forward time-series InSAR technology (such as SBAS, PS, etc.), which can effectively improve the acquisition accuracy of long-time series surface deformation information (Samsonov et al., 2013).

At present, the identification of coal mining subsidence area is to extract suspected surface subsidence area based on a large number of SAR image data and the surface deformation rate obtained by time-series InSAR technology. The extraction efficiency of the surface subsidence area is low, so it is difficult to find the potential surface subsidence area in time. Therefore, it is necessary to propose a new automatic detection and identification method of coal mining subsidence area based on InSAR data results.

Deep learning provides the possibility to process a large amount of data information, and can provide an effective model based on a large number of training data to realize the automatic detection and recognition of a large number of data. Some scholars have begun to try to apply deep learning methods to the monitoring of ground deformation. Guo combined SBAS-InSAR and Yolo model to detect landslides in a high mountainous county (Guo et al., 2022). Yu proposed a lightweight model for subsidence basin detection based on the YOLOv5 network, significantly reducing model parameters while enhancing model accuracy (Yu et al., 2022). Guo proposed a novel method combining YOLOv8 model with InSAR methods to automatically high-precision detect subsidence funnels in mining areas within large-scale regions (Guo et al., 2024).

In this paper, the YOLOv11 model is applied to the automatic detection and identification of coal mining subsidence area, so as to improve the detection efficiency and accuracy of surface subsidence area. A mining area in Shanxi Province was used for experimental research, SAR image data in the study area was collected to extract differential interferogram, and model training and testing were carried out based on YOLOv11 model. Finally, the experimental results are discussed and analyzed.

# 2. Study Area

Shanxi Province is located in northern China, bordering the Inner Mongolia Autonomous Region to the north by the Great Wall, Shaanxi Province to the west by the Yellow River, Hebei Province to the east by the Taihang Mountains, and Henan Province to the south. Shanxi is distributed with rich mineral resources and is a large province for resource development and utilization, occupying an important position in China's mining economy. Among them, there are 270,901 million tons of coal reserves, accounting for 17.3 per cent of the country's reserves and ranking third in the country (Wu et al., 2021).

Yangquan City is located in the east wing of central Shanxi Province, with geographic coordinates 112° 5′ ~114° 4′ E, 37° 40′ ~38° 31′ N. It is situated on the west side of the central Taihang Mountains, and is connected to Dingxiang County and Wutai County of Xinzhou City in the north, and Pingshan County and Jingfu County of Shijiazhuang City and

Jingfuzhe County of Hebei Province in the east, and connected to Xiyang County of Jinzhong City in the south, and next to Jinzhong City Shouyang County, Taiyuan City, Yangqu County; north-south length of about 106 kilometers, east-west width of about 42 kilometers.

Yangquan City is an important mineral concentration area in the country, rich in mineral resources, a long history of development, known as the "hometown of coal and iron" reputation. Proven deposits of up to 52 kinds of minerals, especially anthracite, sulfurous iron ore, bauxite reserves, high grade, easy to mine and known in the world, is one of China's largest anthracite production base, one of the country's three major bauxite production base and one of the five major sulfurous iron ore production base (Xia et al., 2023).

Sentinel-1, an Earth observation satellite launched by the Copernicus Programme of the European Space Agency (ESA), carries a C-band synthetic aperture radar (SAR) that provides all-weather, all-day surface observations. Sentinel 1 has a wide range of applications, including polar environmental monitoring, surface deformation monitoring, forest monitoring, water resource management, agricultural monitoring, urban monitoring and sea ice monitoring.

In this paper, a Sentinel-1 image is selected for experimental study, and the image is cropped according to the administrative area of Yangquan City to obtain a SAR image coverage area of about 10,000 square kilometers. The location of study area is shown in Figure 1.

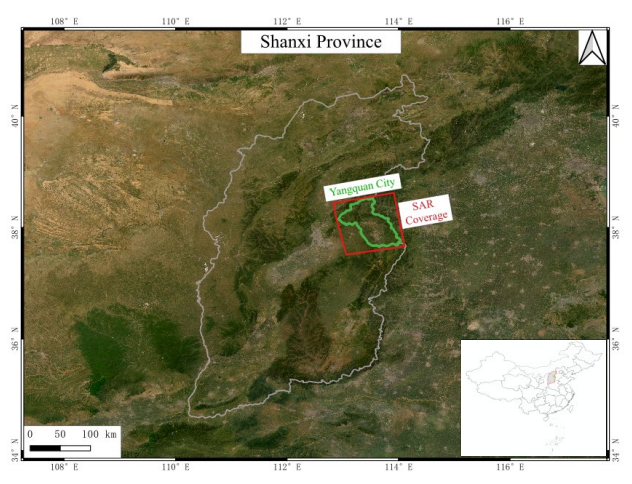


Figure 1. Location of study area.

# 3. Methodology

The technology roadmap used in this article is shown in the Figure 2. First, the SAR images in the study area are processed and the differential interference fringe patterns of each image pair are extracted. Based on the limited interferogram data, the surface subsidence area is identified manually and marked with samples. The marked difference interferogram is cropped to make a uniform size sample data set. The limited sample data set was used for model training and testing to obtain the optimal model, which was used for automatic detection and identification of coal mining subsidence area near the study area, and the detection accuracy of the model was analyzed.

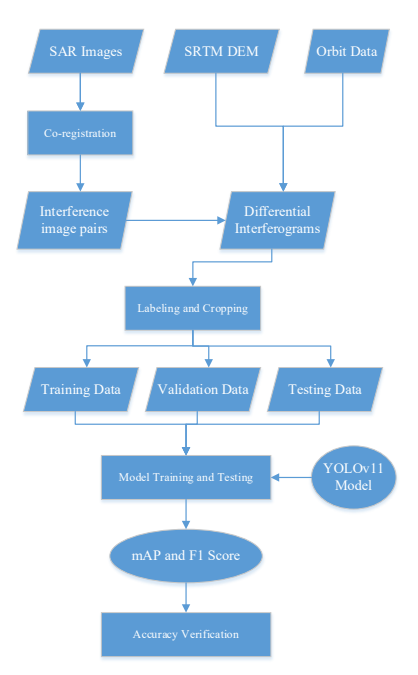


Figure 2. The technology roadmap.

## 3.1 SAR Data Processing

A total of 50 Sentinel-1 SAR image data covering a mining area in Yangquan City were collected in this paper. Take an image as the main image, and register the other slave images to the main image. In this experiment, the time baseline was set to 60 days, interference image pairs were established, and a total of about 120 image pairs were obtained. SRTM 30m DEM and Satellite orbit data are used to remove the topographic phase of the interference image pair to extract the differential interferograms. Among them, 80% of the differential interferograms are selected to make the training and verification sample set, and the remaining 20% are used as the test data set.

The differential interferogram of the training and verification samples was manually marked with the coal mining settling area. The coal mining settlement area in the interferogram is marked as "insar", as shown in Figure 3. At the same time, the data set is enhanced to increase the sample size. The sample set is rotated at 8 different angles between 0 and 90 degrees, and the sample set is scaled, flipped horizontally and vertically. Finally the marked interferogram was cropped to make 512 size samples for subsequent model training and testing. In the end, the obtained model training samples are about 10,000, the verification samples are about 2,000, and the test samples are about 1,000, which are used for the model training and testing in this paper.

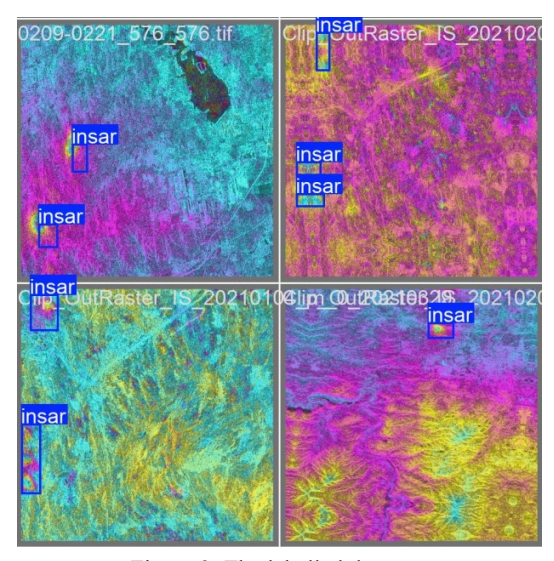


Figure 3. The labelled data set.

### 3.2 YOLOv11 Model Training and Testing

YOLOv11 is the latest generation of object detection algorithms developed by Ultralytics, building upon significant architecture and training method improvements from its predecessors. This version aims to provide higher accuracy, faster speed, and broader support for various visual AI tasks.

The YOLOv11 model continues to balance accuracy and efficiency while performing real-time object detection. Based on previous versions of YOLO, YOLO 11 features significant architectural and training improvements. The most significant architectural changes to improve performance while maintaining speed are the addition of the C3K2 block, the SPFF module, and the C2PSA block. The model is shown in Figure 4. The C3K2 block is an enhancement to the CSP (Cross Stage Part) block introduced in previous versions. This block optimizes the extraction of more complex features using different kernel sizes (e.g. 3x3 or 5x5) and channel separation strategies. The SPFF (Spatial Pyramid Pooling Fusion) module is an optimized version of the SPP (Spatial Pyramid Pooling) module used in the YOLO version. This block enables better model execution by capturing object properties at different scales. The C2PSA block provides more efficient feature extraction by combining channel and spatial information. It also works with the multiple attention mechanism to enable more accurate perception of objects. It optimizes the feature maps of the previous layers and enriches them using the attention mechanism to improve the performance of the model. This structure enables more accurate detection, especially in complex scenes, and improves the accuracy of YOLOv11.

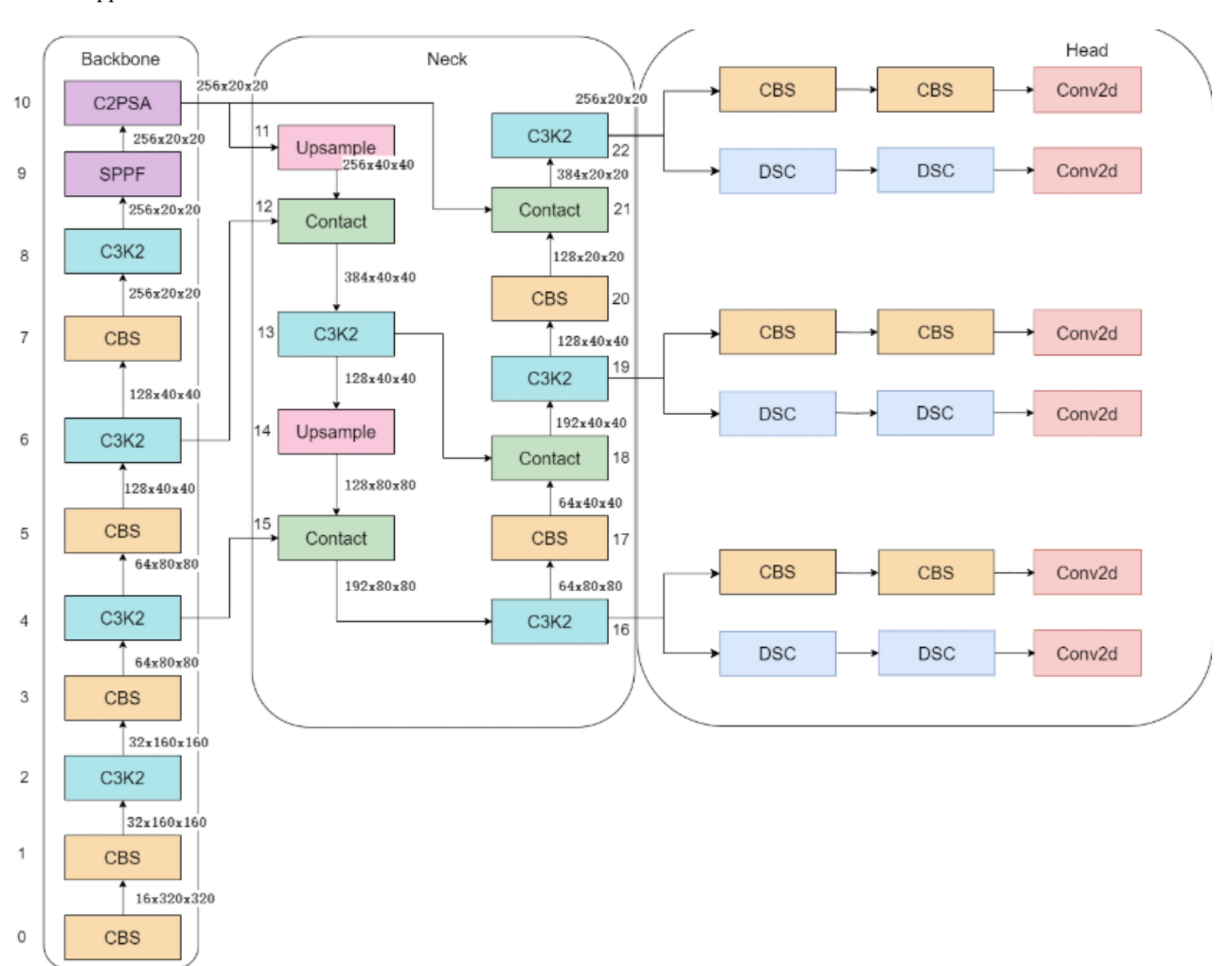


Figure 4. YOLOv11 Model.

YOLOv11 supports a variety of visual AI tasks, including but not limited to object detection, segmentation, pose estimation, tracking, and classification. It continues to employ an efficient Convolutional Neural Network (CNN) structure, which helps in improving processing speed and reducing latency. Compared with the previous YOLO model, the YOLOv11 model has the following advantages: 1) Significantly improved accuracy compared to previous versions. 2) Maintains the real-time advantage of the YOLO series, enabling efficient detection even in complex scenarios. 3) Capable of handling a large number of bounding boxes, such as up to 8400, making it suitable for complex multi-object detection tasks.

The input data of the model is 512X512 interferogram sample set, and the output is the confidence value between the external rectangular box and the target along the settlement region. YOLOv11 model was trained and tested on a computer equipped with an Intel Xeon w7-3455 and an NVIDIA RTX A6000 graphics card. PyTorch was used as the experimental deep learning framework, with CUDA 11.8 for GPU parallel computing and GPU acceleration. The initial learning rate for training was set to 1e-4. The mini-batch size was set to 8 and the training iteration number was set to 200.

According to the model training results, the optimal model weight is selected to detect the coal mining subsidence area automatically on the test data set, and the target detection accuracy of the model in different regions is analyzed.

#### 3.3 Accuracy Verification

In order to evaluate the accuracy of detection and identification of coal mining subsidence area by this model, mAP and F1 index were used to verify the accuracy of the model prediction results.

Mean Average Precision (mAP) is a widely used metric in object detection and information retrieval tasks to evaluate the performance of a model. It provides a single-figure summary that combines both precision and recall across different classes or categories. A higher mAP indicates better overall performance, with a perfect score being 1.0. mAP balances the trade-off between precision and recall, providing a comprehensive measure of the model's ability to detect objects

accurately and comprehensively. The mAP is the mean of the APs across all classes. If there are N classes, the mAP is calculated as:

$$mAP = \frac{1}{N} \sum_{i=1}^{N} AP_i$$
 (1)

where  $AP_i$  = the Average Precision for the i-th class.

F1 Score, also known as the F1 measure or F-score, is a statistical measure that combines precision and recall into a single metric. It is particularly useful in scenarios where there is an uneven class distribution, and it provides a balance between the two metrics. The F1 Score ranges from 0 to 1, with 1 being the best possible score, indicating perfect precision and recall. The F1 Score gives equal weight to both precision and recall, making it a balanced measure. It is especially useful when you need to balance the trade-off between false positives and false negatives. The F1 Score is the harmonic mean of precision and recall, which can be calculated using the following formula:

F1 Score=
$$2 \times \frac{\text{Precision} \times \text{Recall}}{\text{Precision} + \text{Recall}}$$
 (2)

where 
$$\begin{split} &\text{Precision} = \frac{TP}{TP + FP} \text{ , it measures the accuracy of } \\ &\text{positive predictions, the ratio of true positive results (TP) to the total number of positive predictions (TP + FP).} \\ &\text{Recall} = \frac{TP}{TP + FN} \text{ , it measures the ability of the model to find } \\ &\text{all the relevant cases, the ratio of true positive results (TP) to the total number of actual positive instances (TP + FN).} \end{split}$$

# 4. Results and Discussion

In this paper, based on the sample data set made above, YOLOv11 model is adopted for model training, and the optimal model obtained is the training model obtained by the 134th epoch. The result curve of model training is shown in the Figure 5

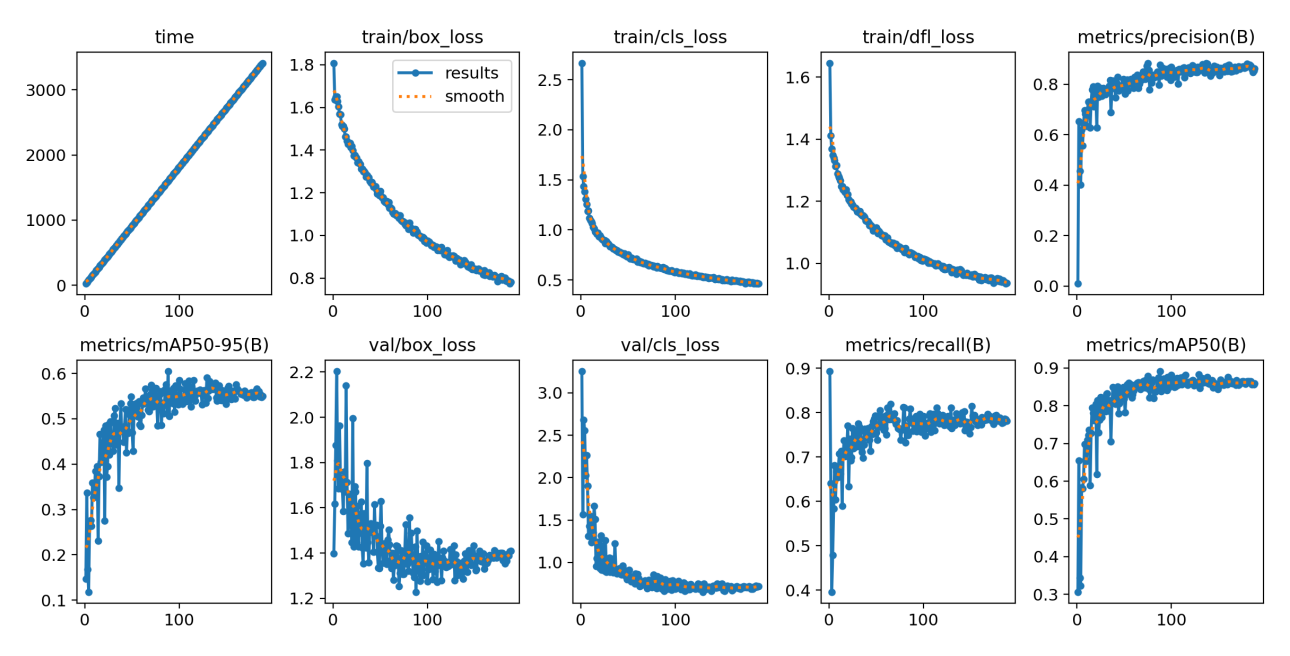


Figure 5. Model training result curves.

As shown in Figure 5, this image consists of multiple subplots that display various metrics over time. Train/Box Loss (train/box loss) shows thhe loss starts high and decreases over time, indicating that the model is learning and improving. The solid blue line represents the actual loss values, while the dotted orange line represents a smoothed version of the loss. Train/Class Loss (train/cls loss) shows the training class loss over time. Similar to the box loss, the class loss starts high and decreases over time, indicating improvement in classification accuracy. Metrics/Precision (metrics/precision(B)) shows the recision starts low and increases over time, indicating that the model is becoming more accurate in its predictions. Metrics/mAP50-95 (metrics/mAP50-95(B)) shows the mean Average Precision (mAP) over time, ranging from 50% to 95% confidence levels and the mAP increases over time, indicating that the model is improving in its ability to detect objects accurately. Metrics/Recall (metrics/recall(B)) shows the recall starts low and increases over time, indicating that the model is becoming better at detecting all relevant instances. Metrics/mAP50 (metrics/mAP50(B)) shows the mean Average Precision (mAP) over time at a 50% confidence level and the mAP increases over time, indicating that the model is improving in its ability to detect objects accurately at this confidence level.

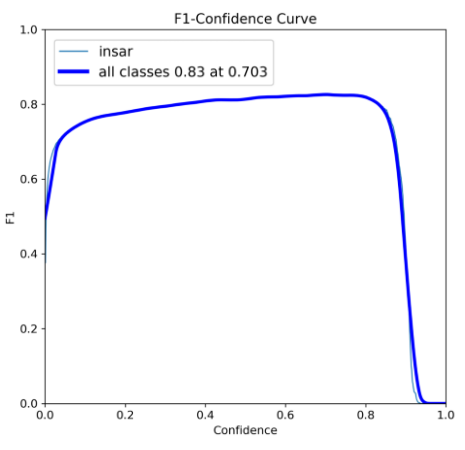


Figure 6. F1-score curve.

Figure 6 depicts the relationship between the F1 score and confidence level, titled "F1-Confidence Curve." The plot includes two curves: 1) Blue Curve (insar): This curve represents the F1 score for the "insar" class across different confidence thresholds. 2) Dark Blue Curve (all classes 0.83 at 0.703): This curve represents the overall F1 score across all classes, with a peak F1 score of 0.83 at a confidence threshold of 0.703. At low confidence levels (close to 0), the F1 score rapidly increases. Between confidence levels of approximately 0.2 to 0.8, the F1 score remains relatively high and stable, close to 0.8. As the confidence level approaches 1, the F1 score drops sharply, approaching 0. This indicates that the model performs best within a moderate range of confidence levels, with the optimal performance occurring at a confidence threshold of 0.703, where the F1 score reaches its peak of 0.83. This suggests that a confidence threshold of around 0.703 is an ideal choice for balancing precision and recall.

Several groups of SAR interferogram were selected for model testing, and part of the test results were shown in Figure 7. The image contains several blue bounding boxes with labels indicating "insar" followed by a numerical value. These values likely represent the coherence or confidence level of the InSAR measurements in those specific regions. The numerical values range from 0.36 to 0.86, with higher values indicating higher coherence and thus more reliable measurements. Areas with high coherence (e.g., 0.86) are likely to be stable or have minimal deformation, while areas with lower coherence (e.g., 0.36) may have experienced significant changes or have inherent noise. The distribution of coherence values can help identify regions of interest for further analysis, such as areas with potential ground deformation. Regions with high coherence values (e.g., 0.86) are likely stable and have reliable InSAR measurements. Regions with low coherence values (e.g., 0.36) may have experienced significant changes or have high noise levels.

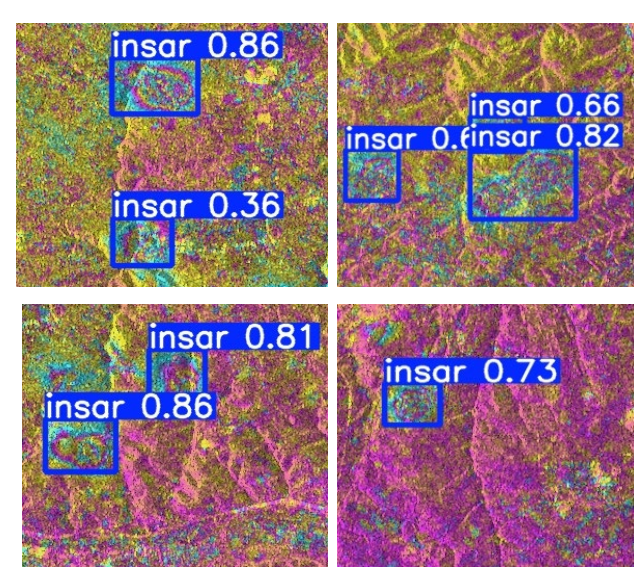


Figure 7. Model testing results.

### 5. Conclusion

In this paper, we applied YOLOv11 model for the first time to the automatic identification of subsidence area in mining area, and achieved good research results. By training YOlOv11 model with limited SAR interferogram, an AI model suitable for automatic identification of subsidence area in Shanxi mining area is obtained.

Although the recognition effect of this paper is good, there are still some problems as follows. 1) The current model has only been tested in Shanxi mining area and has not been tested in more mining areas. The model will be applied to other mining areas to test the accuracy of the model in the future. 2) Currently, the sample data used only uses SAR interferogram. In the future, more types of data will be applied, such as DEM, terrain and other data, to improve the identification accuracy and generalization of the model for mining areas. 3) The YOLOv11 model will also be applied to surface deformation caused by landslides and earthquakes in the future, so as to improve the identification efficiency of geological disasters and reduce the possible human and property losses caused by ground disasters.

## References

Chen, S.W., Wang, X.S., Sato, M., 2016. Urban damage level mapping based on scattering mechanism investigation using fully polarimetric SAR data for the 3.11 East Japan earthquake. IEEE Trans. Geosci. Remote Sens., 54(12), 6919–6929. doi.org/10.1109/TGRS.2016.2588325.

Fan, H.D., Lu, L., Yao, Y., 2018. Method combining probability integration model and a small baseline subset for time series monitoring of mining subsidence. *Remote Sens.*, 10(9), 1444. doi.org/10.3390/rs10091444.

Hu, B., Wang, H.S., Sun, Y.L., Hou, J.G., Liang, J. 2014. Long-term land subsidence monitoring of Beijing (China) using the small baseline subset (SBAS) technique. Remote Sens., 6(5), 3648–3661. doi.org/10.3390/rs6053648.

Guo, H.J., Yi, B.J., Yao, Q.X., Gao, P., Li, H., Sun, J.X., Zhong, C., 2022. Identification of Landslides in Mountainous Area

with the Combination of SBAS-InSAR and Yolo Model. *Sensors*, 22, 6235. doi.org/10.3390/s22166235.

Guo, J., Zhang, Z.J., Wang, M.M., Ma, P.F., Gao, w., Liu, X.G., 2024. Automatic Detection of Subsidence Funnels in Large-Scale SAR Interferograms Based on an Improved-YOLOv8. Model. *IEEE Trans. Geosci. Remote Sens.*, 62. doi.org/10.1109/TGRS.2024.3421662

Ma, P., Lin, H., Wang, W., Yu, H., Chen, F., Jiang, L., Zhou, L., Zhang, Z., Shi, G., Wang, J. 2021. Toward Fine Surveillance: A review of multitemporal interferometric synthetic aperture radar for infrastructure health monitoring. *IEEE Geosci. Remote Sens. Mag.*, 10(1), 207-230. doi.org/10.1109/MGRS.2021.3098182

Samsonov, S., D'Oreye, N., Smets, B., 2013. Ground deformation associated with post-mining activity at the French-German border revealed by novel InSAR time series method. *Int. J. Appl. Earth Observ. Geoinf.*, 23, 142–154. doi.org/10.1016/j.jag.2012.12.008.

Wu, W., Zhou, J., Niu, J., Lv, H. 2021. Study on coupling between mineral resources exploitation and the mining ecological environment in Shanxi Province. *Environ Dev Sustain*, 23(9), 13261-13283. doi.org/10.1007/s10668-020-01209-8.

Xia, Y., Xia, F., Hui, Z., Li, H., Wan, R., Ai, J. 2023. Combined PS-InSAR Technology and High-Resolution Optical Remote Sensing for Identifying Illegal Underground Mining in the Suburb of Yangquan City, Shanxi Province, China. *Remote Sens.* 15, 3565. doi.org/10.3390/rs15143565.

Xue, D., Wang, J., Zhao, Y., Zhou, H. 2012. Quantitative determination of mining-induced discontinuous stress drop in coal. *Int. J. Rock Mech. Mining Sci.*, 111, 1–11. doi.org/10.1016/j.ijrmms.2018.08.003.

Yu, Y., Wang, Z., Li, Z., Ye, K., Li, H., Wang, Z., 2022. A lightweight anchor-free subsidence basin detection model with adaptive sample assignment in interferometric synthetic aperture radar interferogram. *Frontiers Ecology Evol.*, 10, 1–10. doi.org/10.3389/fevo.2022.840464.

Zhang, Z., Wang, C., Tang, Y., Fu, Q., Zhang, H., 2015. Subsidence monitoring in coal area using time-series InSAR combining persistent scatterers and distributed scatterers. *Int. J. Appl. Earth Observ. Geoinf.*, 39, 49–55. doi.org10.1016/j.jag.2015. 02.007.